HHS Public Access

Author manuscript

Nat Med. Author manuscript; available in PMC 2015 September 01.

Published in final edited form as:

Nat Med. 2015 March ; 21(3): 231–238. doi:10.1038/nm.3799.

Targeting EZH2 methyltransferase activity in *ARID1A* mutated cancer cells is synthetic lethal

Benjamin G. Biter[1], **Katherine M. Aird**[1], **Azat Garipov**[1], **Hua Li**[1], **Michael Amatangelo**[1], **Andrew V. Kossenkov**[2], **David C. Schultz**[3], **Qin Liu**[6], **Ie-Ming Shih**[4], **Jose R. Conejo-Garcia**[5], **David W. Speicher**[2,6], and **Rugang Zhang**[1,*]

[1] Gene Expression and Regulation Program, The Wistar Institute, Philadelphia, PA, USA

[2] Center for Systems and Computational Biology, The Wistar Institute, Philadelphia, PA, USA

[3] Center for Chemical Biology and Translational Medicine, The Wistar Institute, Philadelphia, PA, USA

[4] Department of Pathology, Oncology, and Gynecology and Obstetrics, Johns Hopkins Medical Institutions, Baltimore, MD, USA

[5] Tumor Microenvironment and Metastasis Program, The Wistar Institute, Philadelphia, PA, USA

[6] Molecular and Cellular Oncogenesis Program, The Wistar Institute, Philadelphia, PA, USA

Abstract

ARID1A, a chromatin remodeler, shows one of the highest mutation rates across many cancer types. Notably, *ARID1A* is mutated in over 50% of ovarian clear cell carcinomas, which currently has no effective therapy. To date, clinically applicable targeted cancer therapy based on *ARID1A* mutational status has not been described. Here we show that inhibition of the EZH2 methyltransferase acts in a synthetic lethal manner in *ARID1A* mutated ovarian cancer cells. *ARID1A* mutational status correlates with response to the EZH2 inhibitor. We identified *PIK3IP1* as a direct ARID1A/EZH2 target, which is upregulated by EZH2 inhibition and contributes to the observed synthetic lethality by inhibiting PI3K/AKT signaling. Significantly, EZH2 inhibition causes regression of *ARID1A* mutated ovarian tumors *in vivo*. Together, these data demonstrate for the first time a synthetic lethality between *ARID1A* mutation and EZH2 inhibition. They indicate that pharmacological inhibition of EZH2 represents a novel treatment strategy for *ARID1A* mutated cancers.

* Corresponding author: Rugang Zhang, Ph.D., Gene Expression and Regulation Program, The Wistar Institute, Room 307B, 3601 Spruce Street, Philadelphia, PA, rzhang@wistar.org.

Author contributions

B.G.B designed and performed all the experiments and analyzed data and wrote the manuscript. K.M.A. contributed to Fig. 5g-i and manuscript writing. A.G. contributed to Fig. 2b,c, H.L. contributed to Supplementary Fig. 4g. M.A. contributed to Supplementary Fig. 2c, f. A.V.K. performed the analysis presented in Fig. 4a,c, D.C.S. contributed to the epigenetic set construction. Q.L. contributed to statistical design and analysis. I.M.S. contributed key reagents. J.R.C. and D.W.S. participated in experimental design. R.Z. conceived the study and wrote the manuscript.

Disclosure of Competing Financial Interest: None.

Introduction

A major discovery of recent cancer genome-wide sequencing studies has been the identification of significant alterations in genes responsible for modifying chromatin structure [1]. ARID1A, a component of the SWI/SNF chromatin-remodeling complex, is among the genes that show the highest mutation rate across multiple cancer types [2]. The SWI/SNF complex remodels nucleosomes to modulate transcription and its inactivation is thought to drive tumorigenesis by altering gene expression [3]. Notably, *ARID1A* is mutated in ~ 57% of ovarian clear cell carcinoma (OCCC) [4,5]. *ARID1A* mutated OCCC are typically characterized by a lack of genomic instability [4,6]. It has been suggested that perturbations in the regulation of epigenetic chromatin remodeling may be able to substitute for genomic instability [3]. These findings suggest that epigenetic mechanisms play a critical role in the disease. Despite the prevalence of genetic mutations of *ARID1A*, a rational therapeutic approach to target cancers with *ARID1A* mutations has not yet been explored.

EZH2, the catalytic subunit of polycomb repressive complex 2, silences gene expression by generating the lysine 27 trimethylation mark on histone H3 (H3K27Me3) by its catalytic SET domain [7]. EZH2 is often overexpressed in OCCC [8]. EZH2 gain-of-function mutations occur in hematopoietic malignancies such as diffuse large B cell lymphoma (DLBCL). Highly specific small molecule EZH2 inhibitors have been developed and the response to EZH2 inhibitors often correlate with gain-of-function mutations in EZH2 (refs. 9-11). EZH2 inhibitors have since entered clinical trials for these diseases. Here we show that inhibition of EZH2 methyltransferase activity acts in a synthetic lethal manner in *ARID1A* mutated cells. Our findings establish a new paradigm for targeting *ARID1A* mutation in cancer by using pharmacological inhibition of EZH2 methyltransferase activity.

Results

EZH2 inhibitor is selective against ARID1A inactivation

Since epigenetic mechanisms may play a critical role in *ARID1A* mutated OCCC, we evaluated a panel of 15 commercially available small molecule inhibitors known to target epigenetic regulators to identify “hits” that selectively inhibit the growth of ARID1A inactivated cells (Supplementary Table 1). Over 90% of the *ARID1A* mutations observed in OCCC are frame-shift or nonsense mutations that result in loss of ARID1A protein expression [4,5,12]. To mimic loss of ARID1A protein expression caused by the vast majority of *ARID1A* mutations [4] and ensure the same genetic background, we performed the screen using *ARID1A* wild type OCCC RMG1 cells with or without shRNA-mediated ARID1A knockdown (Fig. 1a,b and Supplementary Fig. 1a). We performed the screen in 3 dimensional (3D) cultures using Matrigel to more closely mimic the tumor microenvironment [13]. Notably, ARID1A knockdown itself did not significantly affect the growth of RMG1 cells in 3D culture (Supplementary Fig. 1b). We used the doses of each small molecule based on their previously established IC_{50} concentrations (Supplementary Table 2). Diameters of acini formed in 3D culture were measured as a surrogate for cell growth (Fig. 1c). We identified three small molecule inhibitors that significantly and selectively inhibited the growth of ARID1A knockdown cells compared to controls (Supplementary Table 1). GSK126 was the hit with the highest selectivity against ARID1A

knockdown cells (Fig. 1c,d and Supplementary Table 1). We observed a decrease in acini size by GSK126 using two individual shARID1As (Supplementary Fig. 1c-e). GSK126 is a highly selective and potent small molecule inhibitor of EZH2 methyltransferase activity [9]. Notably, ARID1A knockdown did not alter the expression levels of EZH2 or H3K27Me3 (Fig. 1b).

ARID1A mutation correlates with response to EZH2 inhibitor

To validate the initial findings, we utilized four different ovarian cancer cell lines (TOV21G, OVISE, OVTOKO and SKOV3) with known *ARID1A* mutations [4,6]. We observed loss of ARID1A protein expression in these *ARID1A* mutated cell lines (Fig. 2a). There was a dose-dependent decrease in H3K27Me3 levels by GSK126 in *ARID1A* mutated cells (Fig. 2b). A >95% reduction in H3K27Me3 levels was achieved with 5 μM GSK126 (Fig. 2b,c). H3K9Me3, which is generated by different histone methyltransferases such as SUV39H1 and SETDB1 (ref. 14), was not affected by GSK126 (Fig. 2b,c and Supplementary Fig. 1f-h). GSK126 had no appreciable effect on EZH2 expression (Fig. 2b,c) [9]. ARID1A knockdown did not alter the dose-dependent reduction of H3K27Me3 by GSK126 (Supplementary Fig. 1h).

Similar to RMG1 cells, GSK126 treatment resulted in a significant decrease in 3D growth in ARID1A knockdown KK and OVCA429, two additional *ARID1A* wild type OCCC cell lines (Fig. 2d and Supplementary Fig. 1i-l) [15]. Further, GSK126 significantly reduced acini size of all tested cell lines with *ARID1A* mutation, while the effects of GSK126 on the growth of *ARID1A* wild type cell lines were not significant (Fig. 2e). This was not due to the inability of GSK126 to inhibit EZH2 activity in *ARID1A* wild type cells, as GSK126 was equally effective in decreasing H3K27Me3 levels in these cells (e.g., Supplementary Fig. 1j). GSK126 treatment led to a significant reduction in cell number in *ARID1A* mutated but not wild type cells (e.g., Fig. 2f,i and Supplementary Fig. 1m). Similar growth inhibition by GSK126 was observed in conventional 2D cultures determined by cell counting (Supplementary Fig. 1n). Likewise, growth inhibition of *ARID1A* mutated cells was observed using UNC1999 (ref. 16), another EZH2 inhibitor with less selectivity than GSK126 (Supplementary Fig. 1o-q).

To determine whether re-introducing wild type ARID1A in *ARID1A* mutated cells affects sensitivity to GSK126, we ectopically expressed wild type ARID1A in *ARID1A* mutated OVISE and TOV21G OCCC cells. As reported [15], *ARID1A* restoration suppressed the growth of OCCC cells with *ARID1A* mutation (Fig. 2g,h). GSK126 did not further reduce the acini size of ARID1A restored cells (Fig. 2h). The IC_{50} of GSK126 in *ARID1A* mutated cells was ~267 nM (Fig. 2i), which is comparable to what was previously observed in DLBCL with gain-of-function *EZH2* mutation [9]. Restoration of wild type ARID1A caused a ~16-fold increase in IC_{50} of GSK126 compared to controls (Fig. 2i).

To establish that the observed effects are specifically due to inhibition of EZH2 activity, we knocked down EZH2 expression in *ARID1A* mutated cells in combination with GSK126 treatment. Knockdown of EZH2 mimicked the growth inhibition by GSK126 (Supplementary Fig. 2a-f). GSK126 did not significantly further affect the growth of EZH2 knockdown *ARID1A* mutated cells (Supplementary Fig. 2d-f). The observed growth

inhibition by EZH2 knockdown was rescued by wild type EZH2 but not by an enzymatically inactive SET domain deleted EZH2 mutant (Fig. 3a-d) [7]. This supports the notion that the observed growth inhibition depends upon EZH2 methyltransferase activity.

EZH2 inhibition triggers apoptosis in *ARID1A* mutated cells

We stained acini for H3K27Me3 and cell proliferation marker Ki67. GSK126 treatment significantly decreased H3K27Me3 and the percentage of Ki67 positive cells compared to controls (Fig. 3e-g). GSK126 induces apoptosis in DLBCL with gain-of-function *EZH2* mutations [9]. To determine whether GSK126 triggered apoptosis, we stained the acini for cleaved caspase 3, an apoptotic marker. Compared with controls, there was a significant increase in the percentage of cells positive for cleaved caspase 3 in GSK126 treated *ARID1A* mutated cells (Fig. 3h-j). Other apoptotic markers such as Annexin V were also induced by GSK126 (Supplementary Fig. 3).

PIK3IP1 contributes to the observed synthetic lethality

ARID1A and EZH2 respectively belong to the SWI/SNF and polycomb complexes. The antagonistic roles of SWI/SNF and polycomb proteins in gene transcription were initially suggested from genetic studies in *Drosophila* [17]. We sought to determine whether the observed phenotypes are due to changes in gene expression. Microarray analysis of *ARID1A* mutated OVISE cells treated with GSK126 or restored with wild type ARID1A revealed a significant overlap in differentially regulated genes (2.4-fold enrichment, $P = 5.942 \times 10^{-11}$ for overlap in genes regulated by wild type ARID1A restoration and GSK126 treatment) (Fig. 4a). Known ARID1A target genes such as *CDKN1A* [15] were only upregulated by ARID1A restoration. Conversely, known EZH2 target genes such as *TNSF10* (ref. 18) were only upregulated by GSK126. This suggests that the observed effects in EZH2 methyltransferase inhibited *ARID1A* mutated cells are mediated by a previously undefined set of genes that are commonly regulated by both ARID1A and EZH2.

To identify direct EZH2/H3K27Me3 target genes in *ARID1A* mutated cells, we cross-examined genes that were commonly upregulated by ARID1A restoration or GSK126 treatment with a published EZH2/H3K27Me3 chromatin immunoprecipitation followed by next generation sequencing (ChIP-seq) database using *ARID1A* mutated ovarian cancer cells [18] (Fig. 4a). To identify biologically relevant genes, we cross-referenced the genes that are commonly upregulated by ARID1A restoration and GSK126 with a publicly available OCCC gene expression database (Fig. 4a), which compares laser capture micro-dissected (LCM) OCCC specimens with normal human ovarian surface epithelial (HOSE) cells [19]. H3K27Me3 silences gene expression [7]. Therefore, we focused on genes that were commonly upregulated by both GSK126 and wild type ARID1A restoration but downregulated in the LCM OCCC specimens compared to normal HOSE cells (Fig. 4a and Supplementary Table 3).

We chose the *PI3K-interacting protein 1* (*PIK3IP1*) gene for validation for the following reasons: 1) *PIK3IP1* negatively regulates PI3K/AKT signaling [20,21]; 2) *PI3KCA* is often mutated in OCCC, and mutations in *PI3KCA* and *ARID1A* often co-exist in OCCC [22,23]; and 3) PIK3IP1 negatively regulates cell proliferation and promotes apoptosis [20], the phenotypes

observed in GSK126 treated *ARID1A* mutated cells. There was a significant negative correlation between expression of *EZH2* and *PIK3IP1* in the microarray analysis of LCM specimens (Fig. 4b) [19]. Notably, *PIK3IP1* was expressed at significantly lower levels in *ARID1A* mutated compared to wild type OCCCs (Fig. 4c). Thus, we ectopically overexpressed PIK3IP1 and confirmed that PIK3IP1 inhibited PI3K/AKT signaling, suppressed cell growth and induced apoptosis in *ARID1A* mutated cells (Supplementary Fig. 4a-d). *PIK3IP1* expression was significantly upregulated by both wild type ARID1A restoration and GSK126 in *ARID1A* mutated cells (Fig. 4d and Supplementary Fig. 4e). Supporting the notion that the observed upregulation of PIK3IP1 is due to inhibition of EZH2 methyltransferase activity by GSK126, PIK3IP1 upregulation induced by EZH2 knockdown in *ARID1A* mutated cells can be rescued by wild type EZH2 but not by an enzymatically inactive SET domain deleted EZH2 mutant (Supplementary Fig. 4f). *PIK3IP1* expression was not upregulated by GSK126 in *ARID1A* wild type RMG1 cells (Supplementary Fig. 4g), which correlated with the observation that GSK126 did not affect RMG1 cell growth (Fig. 1d).

ChIP analysis revealed a significant decrease in the association of H3K27Me3 with the *PIK3IP1* gene promoter in GSK126 treated *ARID1A* mutated cells compared with vehicle treated controls (Fig. 4e). In addition, ARID1A restoration caused a significant increase in the association of ARID1A with the *PIK3IP1* gene promoter (Fig. 4f). As a control, the association of core histone H3 with the *PIK3IP1* gene promoter was not affected by either GSK126 or ARID1A restoration (Supplementary Fig. 4h). Association of BRG1, the catalytic subunit of ARID1A-containing chromatin-remodeling complex, with the *PIK3IP1* gene promoter was significantly enhanced by ARID1A restoration (Fig. 4f). Consistently, there is evidence to suggest that ARID1A recruits the remodeling complex to its target genes [15,24]. Interestingly, the association of EZH2 with the *PIK3IP1* gene promoter was not decreased by either ARID1A restoration or GSK126 (Fig. 4e,f). Likewise, the association of H3K27Me3 with the *PIK3IP1* gene promoter was not significantly decreased by ARID1A restoration (Fig. 4f). The induction of *PIK3IP1* by ARID1A restoration correlated with RNA polymerase II recruitment to its promoter (Fig. 4f). Although EZH2/H3K27Me3 are predominantly associated with silenced genes, they also localize to active genes [25]. However, these active genes are typically not regulated by EZH2/H3K27Me3 (ref. 25). Together, these data support a model whereby when both ARID1A and EZH2 are present at the *PIK3IP1* gene promoter, ARID1A dominates over EZH2 and drives *PIK3IP1* expression (Supplementary Fig. 4i). Indeed, ARID1A restoration induced *PIK3IP1* expression in *ARID1A* mutated cells (Fig. 4d), and the EZH2 inhibitor did not affect *PIK3IP1* expression in *ARID1A* wild type cells (Supplementary Fig. 4g). When ARID1A is absent, EZH2 silences *PIK3IP1* expression, and when EZH2 methyltransferase activity is suppressed, *PIK3IP1* is expressed (Supplementary Fig. 4i). Consistently, there was no additional increase in PIK3IP1 expression in cells treated with a combination of GSK126 and wild type ARID1A restoration in *ARID1A* mutated cells (Fig. 4g).

ChIP analysis in *ARID1A* wild type cells revealed that both ARID1A and EZH2 are associated with the *PIK3IP1* gene promoter (Fig. 4h). ARID1A knockdown in *ARID1A* wild type cells decreased the association of ARID1A with the *PIK3IP1* gene promoter (Fig. 4h),

which correlated with a decrease in RNA polymerase II's association with the *PIK3IP1* gene promoter (Fig. 4h) and suppression of PIK3IP1 expression (Fig. 4i). There was no decrease in the association of either EZH2 or H3K27Me3 with the *PIK3IP1* gene promoter by ARID1A knockdown (Fig. 4h). Indeed, treatment of ARID1A knockdown cells with GSK126 led to restoration of PIK3IP1 expression in *ARID1A* wild type cells (Fig. 4i).

To determine whether genetic knockdown of *PIK3IP1* rescues the growth inhibition observed in GSK126 treated *ARID1A* mutated cells, two individual shRNAs to *PIK3IP1* that knocked down its expression were used. Knockdown of PIK3IP1 significantly rescued the growth suppression induced by GSK126 in *ARID1A* mutated cells (Fig. 5a-d and Supplementary Fig. 5a-b). Upregulation of cleaved caspase 3 induced by GSK126 in *ARID1A* mutated cells was also significantly suppressed by PIK3IP1 knockdown (Fig. 5e-f and Supplementary Fig. 5c-d).

Since PIK3IP1 suppresses PI3K/AKT signaling (Supplementary Fig. 4a) and PIK3IP1 contributes to the observed effects by GSK126 in *ARID1A* mutated cells (Fig. 5), we sought to determine whether PI3K/AKT signaling affects the sensitivity of *ARID1A* mutated cells to GSK126. We ectopically expressed a constitutively active myristoylated PI3KCA mutant (myrPI3KCA) in the *ARID1A* mutated OVTOKO cell line that does not have mutated *PI3KCA* [6] to increase PI3K/AKT signaling (Fig. 5g). Indeed, the PI3KCA mutant further enhanced the observed growth inhibition by GSK126 (Fig. 5h,i). This supports the notion that the effects of EZH2 inhibition in *ARID1A* mutated cells are due to increased PIK3IP1 expression, an inhibitor of PI3K activity. Consequently, increased PI3K activity results in increased sensitivity to EZH2 inhibition, which resulted in more growth inhibition.

EZH2 inhibitor causes regression of *ARID1A* mutated tumors

GSK126 is a specific EZH2 inhibitor that is well tolerated in immunocompromised mice [9]. We orthotopically injected luciferase-expressing *ARID1A* mutated OVISE cells into the immunocompromised female mouse bursa sac that covers the ovary. The injected cells were allowed to grow for one week to establish tumors. We randomly assigned mice into two groups (n=5/group) and treated mice daily with vehicle control or GSK126 (50 mg/kg) by intraperitoneal injection for an additional three weeks [9]. GSK126 treatment caused regression of the orthotopically transplanted *ARID1A* mutated OVISE cells (Fig. 6a,b). At necropsy, we measured the orthotopically transplanted tumor size. GSK126 treatment significantly decreased the size of the orthotopically xenografted tumors compared with controls (Fig. 6c). Similarly, GSK126 treatment (50 mg/kg) caused regression of orthotopically xenografted *ARID1A* mutated TOV21G tumors after first establishing tumors for four weeks followed by two weeks of treatment (Supplementary Fig. 6a). In contrast, GSK126 treatment did not significantly affect the size of orthotopically xenografted *ARID1A* wild type RMG1 tumors (Supplementary Fig. 6b).

We sought to determine the effects of GSK126 on the dissemination of *ARID1A* mutated OCCC cells, another clinical feature of ovarian cancer [26], in an intraperitoneal xenograft model. We injected *ARID1A* mutated OVISE cells into the mouse intraperitoneal cavity. The injected tumor cells were allowed to grow for 4 days, and the mice were randomized into two groups (n=6/group). Mice were treated daily with GSK126 (50 mg/kg) or vehicle

control via intraperitoneal injection. Compared with controls, GSK126 significantly reduced the number of tumor nodules within the peritoneal cavity after three weeks of treatment (Fig. 6d and Supplementary Fig. 6c).

Immunohistochemical analysis of *ARID1A* mutated tumors treated with GSK126 or vehicle controls revealed that H3K27Me3 staining was decreased by GSK126, while GSK126 did not weaken EZH2 staining (Fig. 6e,f). Further, GSK126 treatment decreased the expression of Ki67 (Fig. 6e,f). There was an increase in PIK3IP1 staining and a decrease in phospho-AKT staining in GSK126 treated tumors (Fig. 6e,f). Consistently, the apoptotic marker cleaved caspase 3 was induced by GSK126 (Fig. 6e,f). In *ARID1A* wild type tumors, although GSK126 decreased H3K27Me3 staining (Supplementary Fig. 6d), it did not affect the expression of Ki67, PIK3IP1, phospho-AKT or cleaved caspase 3 (Supplementary Fig. 6d).

Discussion

The EZH2 inhibitor selectively suppressed the growth of *ARID1A* mutated cells. This was neither due to changes in EZH2 expression nor due to inability of the EZH2 inhibitor to suppress the enzymatic activity of EZH2 in *ARID1A* wild type cells as GSK126 was equally effective in decreasing H3K27M3 levels regardless of *ARID1A* mutation status (Fig. 2). Similarly, in DLBCL, the response to EZH2 inhibitors often correlates with gain-of-function mutations in *EZH2* (refs. 9-11), despite the fact that EZH2 inhibitors are equally effective in reducing the H3K27Me3 levels in *EZH2* wild type cells. A recent study shows that ARID1B is a specific vulnerability in *ARID1A* mutant cancers [27], further highlighting the potential of synthetic lethal strategies for *ARID1A* mutation in cancer.

ARID1A and EZH2 are antagonistic in regulating *PIK3IP1* expression (Fig. 4). We were unable to perform ARID1A ChIP-seq analysis due to lack of a suitable anti-ARID1A antibody. Regardless, we successfully identified *PIK3IP1* as the ARID1A/EZH2 target gene that contributes to the observed synthetic lethality (Fig. 5). In rhabdoid tumors, loss of SNF5, a core subunit of SWI/SNF, directly upregulates EZH2 (ref. 28). Survival of SNF5-deficient cancer cells depends upon the upregulated EZH2, and these cancer cells are sensitive to EZH2 inhibition [28,29]. Here, ARID1A knockdown did not affect EZH2 expression, but sensitized cells to EZH2 inhibition (Fig. 1b, c; 2d and Supplementary Fig. 1i-l). Conversely, wild type ARID1A restoration in *ARID1A* mutated cells conferred resistance to the EZH2 inhibitor while it did not change EZH2 expression (Fig. 2g). Thus, the antagonism between EZH2 and ARID1A occurs at a functional level (Fig. 6g and Supplementary Fig. 4i).

Our studies demonstrate that targeting the EZH2 methyltransferase activity by EZH2 inhibitors in *ARID1A* mutated cells represents a novel synthetic lethal therapeutic strategy. Given that *ARID1A* mutation and loss of expression and genetic alterations in other subunits of ATP-dependent chromatin remodeling complexes are observed at a high frequency in many cancer types [1,30], we anticipate our finding to have far-reaching implications for future epigenetic therapeutic strategies.

Methods

Cell lines and 3D culture conditions

OVISE, TOV21G, RMG1 and OVTOKO cell lines were all obtained from Japanese Collection of Research Bioresources. SKOV3 cell line was obtained from American Type Culture Collection. OVCA429 and KK cell lines were obtained from Dr. Ie-Ming Shih. All cell lines were cultured according to instructions and in 3D conditions using Matrigel unless otherwise specified. All cell lines were used within 6 months of culture after receiving them, but were not tested. 3D culture was adapted from previously published methods [31] using growth factor reduced-Matrigel (GFR-Matrigel; BD Biosciences). In the 3D culture models, GSK126 treatment was started at the time of assay setup. Briefly, a single cell suspension was plated in 8-well chambers covered with Matrigel. Matrigel media with either vehicle control (DMSO) or drug was changed every 4 days and cells were grown for 12 days. Each of the experiments was performed in duplicate in three independent experimental repeats.

Reagents and Antibodies

Small molecules utilized in the screen were all obtained from the Molecular Screening Facility at The Wistar Institute. GSK126 was obtained from Xcess Biosciences and Active Biochem. UNC1999 was obtained from Selleckchem. The following antibodies from the indicated suppliers were used: anti-EZH2 (BD Bioscience, Cat. No: 612666, 1:1000), anti-EZH2 (Cell Signaling, Cat. No: 5246, 1:100), anti-ARID1A (Sigma, Cat. No: HPA005456, 1:1000), anti-H3K27Me3 (Cell Signaling, Cat. No: 9733, 1:1000), anti-β-actin (Sigma, Cat. No: A5441, 1:10,000), anti-ARID1A (Santa Cruz, Cat. No: sc-32761, 1:500), anti-Ki67 (Cell Signaling, Cat. No: 9449, 1:1000), anti-PIK3IP1 (Santa Cruz, Cat. No: sc-86785, 1:500), anti-Histone H3 (Millipore, Cat. No: 06-755, 1:1000), anti-GAPDH (Millipore, Cat. No: MAB374, 1:10,000), anti-cleaved caspase 3 (Cell Signaling, Cat. No: 9661, 1:10,000), anti-PI3K (p110alpha) (Cell Signaling, Cat. No: 4255, 1:1000), anti-pAKT (T308, Cell Signaling, Cat. No: 13038, 1:1000), anti-AKT (Cell Signaling, Cat. No: 9272, 1:1000) and anti-H3K9Me3 (Abcam, Cat. No: ab8898, 1:1000). pBabe-Myr-PIK3CA143V plasmid was obtained from Addgene. pBabe-EZH2, pBabe-EZH2 ΔSET and pQCXIP-PIK3IP1 plasmids were generated by standard molecular cloning protocols, and details are available upon request. Growth factor reduced Matrigel was purchased from BD Bioscience.

Lentivirus infection

pLenti-CMV-Puro-Luciferase was obtained from Addgene. pLKO.1-shARID1As (TRCN0000059090 and TRCN0000059089), pLKO.1-shEZH2 (TRCN0000040073), pLKO.1-shPIK3IP1 (#1 TRCN0000133982, #2 TRCN0000135363 and #3 TRCN0000138560) were obtained from the Molecular Screening Facility at The Wistar Institute. Lentivirus was packaged using the Virapower Kit from Invitrogen (Carlsbad, CA) following the manufacturer's instructions as described previously [8,32,33].

Microarray, database and bioinformatics

ARID1A mutated OVISE cells expressing an inducible wild type ARID1A [15] were plated on Matrigel and treated with DSMO, 1μg/mL doxycycline to induce wild type ARID1A

expression, or 5μM GSK126. Cells were recovered from 3D culture and RNA was extracted with Trizol (Invitrogen) and subsequently cleaned and DNase treated using RNeasy columns (Qiagen). Eukaryote total RNA nano Bioanalyzer (Agilent) assay was used to confirm the quality of RNA, and all RNA used for next steps had an RIN>8.6. cDNA made from the RNA was hybridized to Illumina Bead Array HumanHT-12 v4 by Wistar Genomics Facility (Whole human genome). Images were analyzed and expression changes were evaluated in Illumina Genome Studio. Illumina GenomeStudio software was used to export expression levels and detect *P*-values for each probe of each sample. Signal intensity data was quantile normalized and probes that showed an insignificant detection p-value (p>0.05) in all samples were removed from further analysis. Pair-wise group comparisons were done using paired SAM test [34] and correction for multiple testing to estimate False Discovery Rate (FDR) was done with the Storey et al. procedure [35]. Differentially expressed genes in the ARID1A restored sample were overlapped with GSK126 differentially expressed genes and the significance of overlap was calculated using the hypergeometric test. We used statistical methods for defining significantly changed genes with FDR of 10% as a cutoff plus $P<0.05$ for overlap. All microarray data can be found at Gene Expression Omnibus (GEO) database (GEO access number: GSE54979).

Gene expression microarray data sets for 10 cases of laser capture and microdissected ovarian clear cell carcinomas and 10 individual isolations of normal human ovarian surface epithelial cells were obtained from Gene Expression Omnibus (GEO) (http://www.ncbi.nlm.nih.gov/geo/) (GEO accession number: GSE29450) [19]. EZH2/H3K27Me3 ChIP-seq in *ARID1A* mutated ovarian cancer SKOV3 cells was obtained through published data [18]. RNA-seq data for *ARID1A* wild type or mutated OCCC specimens was obtained from European Genome-Phenome Archive [4]. Only samples with comparable 50bp length reads data were analyzed. Sample CCC66 was not considered for analysis due to low number of reads (<50% of median number of reads across all samples). Bowtie2 (ref. 36) was used for alignment against hg19 version of human genome and Tophat2 (ref. 37) was used to estimate RPKM expression values for each gene transcript in each sample using transcript information from UCSC database. ARID1A positive samples without mutation were assigned to *ARID1A* wild type group ($n=5$, includes CCC67, CCC69, CCC71, CCC72 and CCC73) and ARID1A negative samples with mutation were assigned to *ARID1A* mutated group ($n=4$, includes CCC02, CCC04, CCC14 and CCC14). Two-tailed unpaired *t*-test was used to compare the two groups.

Annexin V staining for detecting apoptotic cells (Guava assay)

Phosphatidylserine externalization was detected using an Annexin V staining kit (Millipore) following the manufacturer's instructions. Annexin V–positive cells were detected using the Guava System and analyzed with the Guava Nexin software Module (Millipore).

Reverse-Transcriptase quantitative PCR (RT-qPCR)

RNA was extracted from cells with Trizol (Life Technologies) and DNase treated using RNeasy columns (Qiagen). Expression of mRNA levels for *PIK3IP1* (Fwd 5'-GCTAGGAGGAACTACCACTTTG-3' and Rev 5'-GATGGACAAGGAGCACTGTTA-3'), *EZH2* ORF (Fwd 5'-

GACGGCTTCCCAATAACAGTA-3' and Rev 5'-AGTGCCAATGAGGACTCTAAA-3'), and *EZH2* 3'UTR (Fwd 5'-AATCCCTTGACCTCTGAAAC-3' and Rev 5'-ACTGGTACAAAACACTTTGC-3') was determined using SYBR green iScript (Bio-Rad) master mix on a Bio-Rad Chromo4 machine. β-2-microglobulin was used as an internal control.

Immunofluorescence and immunohistochemical staining

Immunofluorescence was performed on day 8 or 12 as indicated by fixing samples in 2% paraformaldehyde and permeabilizing in 2% paraformaldehyde with 0.5% Triton-X. Samples were incubated with primary antibodies for 2 hours at room temperature, highly cross absorbed secondary antibodies (Invitrogen) for 1 hour at room temperature and mounted with prolong anti-fade reagent (Invitrogen). Immunostained acini were then imaged using a Leica Confocal microscope. Immunohistochemical staining was performed as we have described previously [38] on consecutive sections from xenografted tumors dissected from control or GSK126 treated immunocompromised nude female mice.

Intraperitoneal and intrabursal orthotopic xenograft models *in vivo*

The protocols were approved by the Institutional Animal Care and Use Committee (IACUC). For the intraperitoneal model, 3×10^6 OVISE cells were injected intraperitoneally into 6-8-week- old female immunocompromised nude mice. On day 4 after injection, mice were randomized into vehicle control (captisol) and GSK126 treatment at 50 mg/kg daily for additional 26 days (n=6 mice per group). At the end of experiments (day 30), mice were sacrificed, and formation of tumor nodules in the peritoneal cavity was examined. Intrabursal orthotopic xenograft was performed as described previously [38,39]. Briefly, 1×10^6 luciferase-expressing *ARID1A* mutated OVISE cells were unilaterally injected into the ovarian bursa sac of 6-8 weeks old female immunocompromised nude mice (n=5 per group). For *in vivo* experiments, the sample size of 5 mice per group was determined based on the data shown from *in vitro* experiments. The effect size (defined as the difference of means divided by standard deviation) is observed as large as 2.9 in our *in vitro* data. To be conservative, for *in vivo* experiments, we expected to see an effect size of at least 2.0. In order to have more than 80% power to detect an effect size of 2.0 or larger at a two-sided statistical significance level, 5 mice per group would be required. The *in vivo* experimental data reflect an effect size of 2.7, which is consistent with our hypothesis. One week after injection, tumors were visualized by injecting luciferin (i.p.; 4 mg/mice) resuspended in PBS and imaged with an IVIS Spectrum imaging system. The mice were then randomized into two groups based on luciferase activity and treated with vehicle control (captisol) or GSK126 50 mg/kg daily for additional 3 weeks and imaged weekly for luciferase activity. Images were analyzed using Live Imaging 4.0 software. Imaging analysis was performed blindly but not randomly. At the end of the experiments (day 30), tumors were surgically dissected and the sizes of ovary from both injected side and counter lateral side were measured. The tumor size was calculated by subtracting the control side ovary from the tumor cell injected side to limit variations among different mice. For intrabursal orthotopic xenografts using *ARID1A* mutated TOV21G or *ARID1A* wild type RMG1 cells, the same procedure was used except first establishing the tumors for 4 weeks before treating the

randomized mice with vehicle control (captisol) or GSK126 50 mg/kg daily for additional 2 weeks.

Chromatin Immunoprecipitation (ChIP)

ChIP was performed as we have previously described [33]. The following antibodies were used to perform ChIP: anti-H3K27Me3 (Cell Signaling, Cat. No: 9733), anti-ARID1A (Santa Cruz, Cat. No: sc-32761), anti-BRG1 (Santa Cruz, Cat. No: sc-10768), anti-RNA polymerase II (Santa Cruz, Cat. No: sc-899) or anti-EZH2 (Cell Signaling, Cat. No: 5246). An isotype matched IgG was used as a negative control. ChIP DNA was analyzed by quantitative PCR against the promoter of the human *PIK3IP1* gene using the following primers: Forward: 5'-CACATTGA-GCTGGTGTTTGTT-3' and Reverse: 5'-CCATTGCCACTTCAAAGAGTTT-3'.

Statistical analysis

Statistical analyses were performed using GraphPad Prism 5 (GraphPad) for Mac OS. Quantitative data are expressed as mean ± s.e.m. unless otherwise stated. Spearman's test was used to measure statistical correlation. For all statistical analyses, the level of significance was set at 0.05.

Supplementary Material

Refer to Web version on PubMed Central for supplementary material.

Acknowledgement

We thank Drs. Dario Altieri, Maureen Murphy and Ramin Shiekhattar for critical comments and Mr. Xiang Hua and Ms. Youngran Park for technical assistance. This work was supported by US National Institutes of Health/National Cancer Institute grants (R01CA160331 and R01CA163377 to R.Z.), a US Department of Defense ovarian cancer academy award (OC093420 to R.Z.) and an Ovarian Cancer Research Fund program project (to R.Z.). R.Z. is an Ovarian Cancer Research Fund Liz Tilberis Scholar. B.G.B. is supported by an American Cancer Society postdoctoral fellowship (PF-13-058-01-TBE). K.M.A is supported by a US National Institutes of Health/National Cancer Institute training grant (T32CA9171-35). Support of Core Facilities was provided by Cancer Center Support Grant (CCSG) CA010815 to The Wistar Institute.

References

1. Garraway LA, Lander ES. Lessons from the cancer genome. Cell. 2013; 153:17–37. [PubMed: 23540688]
2. Lawrence MS, et al. Discovery and saturation analysis of cancer genes across 21 tumour types. Nature. 2014; 505:495–501. [PubMed: 24390350]
3. Wilson BG, Roberts CW. SWI/SNF nucleosome remodellers and cancer. Nature reviews. Cancer. 2011; 11:481–492. [PubMed: 21654818]
4. Wiegand KC, et al. ARID1A mutations in endometriosis-associated ovarian carcinomas. N Engl J Med. 2010; 363:1532–1543. [PubMed: 20942669]
5. Jones S, et al. Frequent mutations of chromatin remodeling gene ARID1A in ovarian clear cell carcinoma. Science. 2010; 330:228–231. [PubMed: 20826764]
6. Anglesio MS, et al. Type-specific cell line models for type-specific ovarian cancer research. PLoS One. 2013; 8:e72162. [PubMed: 24023729]
7. Cao R, Zhang Y. The functions of E(Z)/EZH2-mediated methylation of lysine 27 in histone H3. Current opinion in genetics & development. 2004; 14:155–164. [PubMed: 15196462]

8. Li H, Cai Q, Godwin AK, Zhang R. Enhancer of zeste homolog 2 promotes the proliferation and invasion of epithelial ovarian cancer cells. Molecular cancer research : MCR. 2010; 8:1610–1618. [PubMed: 21115743]
9. McCabe MT, et al. EZH2 inhibition as a therapeutic strategy for lymphoma with EZH2-activating mutations. Nature. 2012; 492:108–112. [PubMed: 23051747]
10. Knutson SK, et al. A selective inhibitor of EZH2 blocks H3K27 methylation and kills mutant lymphoma cells. Nature chemical biology. 2012; 8:890–896. [PubMed: 23023262]
11. Qi W, et al. Selective inhibition of Ezh2 by a small molecule inhibitor blocks tumor cells proliferation. Proceedings of the National Academy of Sciences of the United States of America. 2012; 109:21360–21365. [PubMed: 23236167]
12. Guan B, Gao M, Wu CH, Wang TL, Shih Ie M. Functional analysis of in-frame indel ARID1A mutations reveals new regulatory mechanisms of its tumor suppressor functions. Neoplasia. 2012; 14:986–993. [PubMed: 23097632]
13. Yamada KM, Cukierman E. Modeling tissue morphogenesis and cancer in 3D. Cell. 2007; 130:601–610. [PubMed: 17719539]
14. Jenuwein T. The epigenetic magic of histone lysine methylation. FEBS J. 2006; 273:3121–3135. [PubMed: 16857008]
15. Guan B, Wang TL, Shih Ie M. ARID1A, a factor that promotes formation of SWI/SNF-mediated chromatin remodeling, is a tumor suppressor in gynecologic cancers. Cancer research. 2011; 71:6718–6727. [PubMed: 21900401]
16. Konze KD, et al. An orally bioavailable chemical probe of the Lysine Methyltransferases EZH2 and EZH1. ACS chemical biology. 2013; 8:1324–1334. [PubMed: 23614352]
17. Kennison JA, Tamkun JW. Dosage-dependent modifiers of polycomb and antennapedia mutations in Drosophila. Proceedings of the National Academy of Sciences of the United States of America. 1988; 85:8136–8140. [PubMed: 3141923]
18. Li H, et al. ALDH1A1 is a novel EZH2 target gene in epithelial ovarian cancer identified by genome-wide approaches. Cancer Prev Res (Phila). 2012; 5:484–491. [PubMed: 22144423]
19. Stany MP, et al. Identification of novel therapeutic targets in microdissected clear cell ovarian cancers. PLoS One. 2011; 6:e21121. [PubMed: 21754983]
20. He X, et al. PIK3IP1, a negative regulator of PI3K, suppresses the development of hepatocellular carcinoma. Cancer research. 2008; 68:5591–5598. [PubMed: 18632611]
21. Zhu Z, et al. PI3K is negatively regulated by PIK3IP1, a novel p110 interacting protein. Biochemical and biophysical research communications. 2007; 358:66–72. [PubMed: 17475214]
22. Yamamoto S, Tsuda H, Takano M, Tamai S, Matsubara O. Loss of ARID1A protein expression occurs as an early event in ovarian clear-cell carcinoma development and frequently coexists with PIK3CA mutations. Modern pathology : an official journal of the United States and Canadian Academy of Pathology, Inc. 2012; 25:615–624.
23. Samartzis EP, Noske A, Dedes KJ, Fink D, Imesch P. ARID1A mutations and PI3K/AKT pathway alterations in endometriosis and endometriosis-associated ovarian carcinomas. International journal of molecular sciences. 2013; 14:18824–18849. [PubMed: 24036443]
24. Chandler RL, et al. ARID1a-DNA interactions are required for promoter occupancy by SWI/SNF. Molecular and cellular biology. 2013; 33:265–280. [PubMed: 23129809]
25. Davidovich C, Zheng L, Goodrich KJ, Cech TR. Promiscuous RNA binding by Polycomb repressive complex 2. Nature structural & molecular biology. 2013; 20:1250–1257.
26. Cho KR, Shih Ie M. Ovarian cancer. Annual review of pathology. 2009; 4:287–313.
27. Helming KC, et al. ARID1B is a specific vulnerability in ARID1A-mutant cancers. Nature medicine. 2014; 20:251–254.
28. Wilson BG, et al. Epigenetic antagonism between polycomb and SWI/SNF complexes during oncogenic transformation. Cancer cell. 2010; 18:316–328. [PubMed: 20951942]
29. Knutson SK, et al. Durable tumor regression in genetically altered malignant rhabdoid tumors by inhibition of methyltransferase EZH2. Proceedings of the National Academy of Sciences of the United States of America. 2013; 110:7922–7927. [PubMed: 23620515]

30. Hargreaves DC, Crabtree GR. ATP-dependent chromatin remodeling: genetics, genomics and mechanisms. Cell research. 2011; 21:396–420. [PubMed: 21358755]

31. Debnath J, Muthuswamy SK, Brugge JS. Morphogenesis and oncogenesis of MCF-10A mammary epithelial acini grown in three-dimensional basement membrane cultures. Methods. 2003; 30:256–268. [PubMed: 12798140]

32. Ye X, et al. Downregulation of Wnt signaling is a trigger for formation of facultative heterochromatin and onset of cell senescence in primary human cells. Mol Cell. 2007; 27:183–196. [PubMed: 17643369]

33. Tu Z, et al. Oncogenic RAS regulates BRIP1 expression to induce dissociation of BRCA1 from chromatin, inhibit DNA repair, and promote senescence. Developmental cell. 2011; 21:1077–1091. [PubMed: 22137763]

34. Zhang S. A comprehensive evaluation of SAM, the SAM R-package and a simple modification to improve its performance. BMC bioinformatics. 2007; 8:230. [PubMed: 17603887]

35. Storey JD, Tibshirani R. Statistical significance for genomewide studies. Proceedings of the National Academy of Sciences of the United States of America. 2003; 100:9440–9445. [PubMed: 12883005]

36. Langmead B, Salzberg SL. Fast gapped-read alignment with Bowtie 2. Nature methods. 2012; 9:357–359. [PubMed: 22388286]

37. Kim D, et al. TopHat2: accurate alignment of transcriptomes in the presence of insertions, deletions and gene fusions. Genome biology. 2013; 14:R36. [PubMed: 23618408]

38. Bitler BG, et al. Wnt5a suppresses epithelial ovarian cancer by promoting cellular senescence. Cancer research. 2011; 71:6184–6194. [PubMed: 21816908]

39. Li H, et al. SUZ12 promotes human epithelial ovarian cancer by suppressing apoptosis via silencing HRK. Mol Cancer Res. 2012; 10:1462–1472. [PubMed: 22964433]

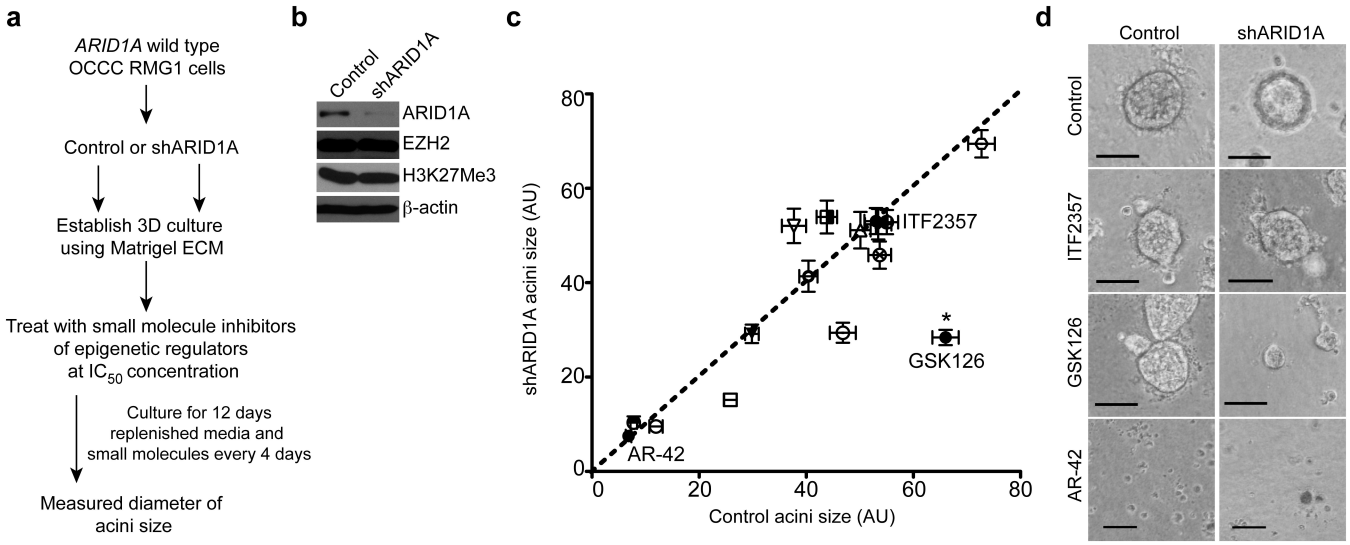

Figure 1.

GSK126, an EZH2 inhibitor, is selective against ARID1A knockdown cells compared with controls. (**a**) Flow-diagram of the evaluation for a panel of epigenetic inhibitors. *ARID1A* wild type OCCC RMG1 cells were transduced with lentivirus encoding a shARID1A or control. Following drug selection, cells were plated onto Matrigel and treated with 15 individual small molecules and vehicle control using IC_{50} concentrations as detailed in Supplementary Table 2. (**b**) Immunoblotting of ARID1A, EZH2, H3K27Me3 and loading control β-actin in the indicated cells. (**c**) Quantification of the average acini diameter (each symbol represents a small molecule) graphed as a scatter plot. The x-axis indicates the acini size formed by control *ARID1A* wild type treated cells, while the y-axis indicates the acini size formed by the same small molecule treated shARID1A-expressing RMG1 cells. * P <0.0001 calculated with two-tailed t test using GraphPad Prism 5 software. Number of acini (n) for each of the small molecules used for analysis is listed in Supplementary Table 1. Error bars represent s.e.m. (**d**) Representative images of acini from indicated small molecules. Scale Bars = 75 of measurable units (AU) using the NIH Image J software. GSK126 (100nM) represents screening hit that selectively inhibits the growth of ARID1A knockdown cells compared with controls. ITF2357 and AR-42 represent small molecule inhibitors that showed no significant effects in growth inhibition and significantly suppressed cell growth regardless of ARID1A status, respectively.

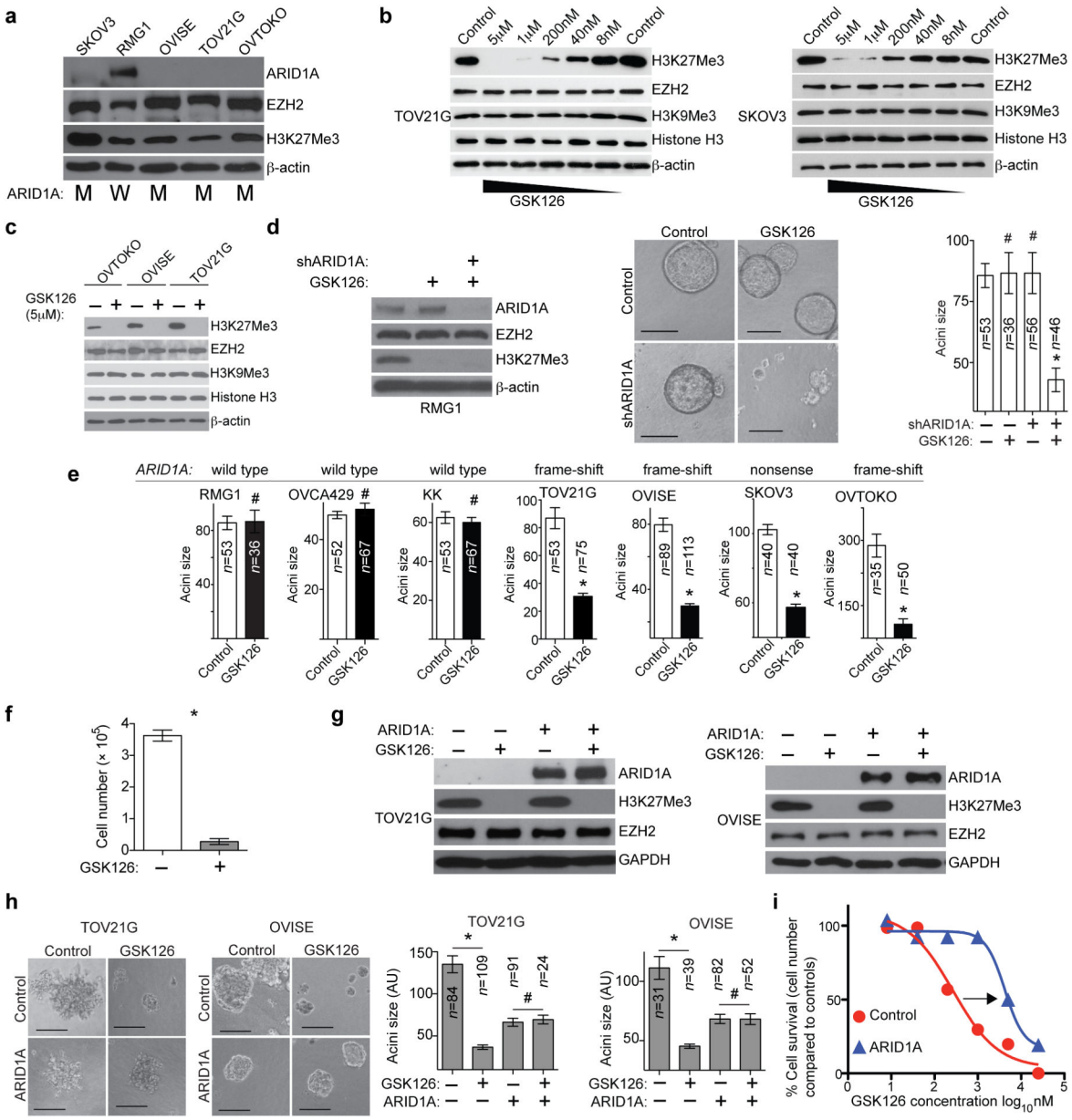

Figure 2.

Response to the EZH2 inhibitor is dependent on ARID1A status. (**a**) Immunoblotting of ARID1A, EZH2, H3K27Me3 and loading control β-actin in the indicated cell lines. *ARID1A* mutation status is indicated as mutated (M) or wild type (W). (**b-c**) Immunoblotting of the indicated proteins following treatment with GSK126 for 72 hours. (**d**) Immunoblotting of the indicated proteins in RMG1 cells expressing shARID1A or control treated with or without 5 μM GSK126. Images of acini formed and the diameter of acini was measured. * $P<0.0001$. (**e**) Quantification of the diameter of acini formed by the indicated cells with or without 5 μM GSK126 treatment in 3D culture for 12 days. # $P=0.914$, * $P<0.0001$. *ARID1A* mutation status is indicated above the graph. (**f**) Quantification of cell numbers for the *ARID1A* mutated OVISE cells. $n=6$, * $P<0.0001$. (**g**) Immunoblotting of the indicated

proteins in *ARID1A* mutated OVISE and TOV21G cells with or without wild type ARID1A restoration treated with or without 5 μM GSK126. (**h**) Acini formation was examined after 12 days in 3D culture and the diameter of acini was measured. # $P>0.05$, * $P<0.0001$. (**i**) Dose response curves of *ARID1A* mutated TOV21G cells with or without wild type ARID1A restoration treated with the indicated dose of GSK126 for 12 days in 3D cultures. Scale bars = 75 AU in NIH Image J software. Number of acini (*n*) is indicated on the graphs as the representative of three experimental repeats. Error bars represent s.e.m. *P* calculated with two-tailed *t* test.

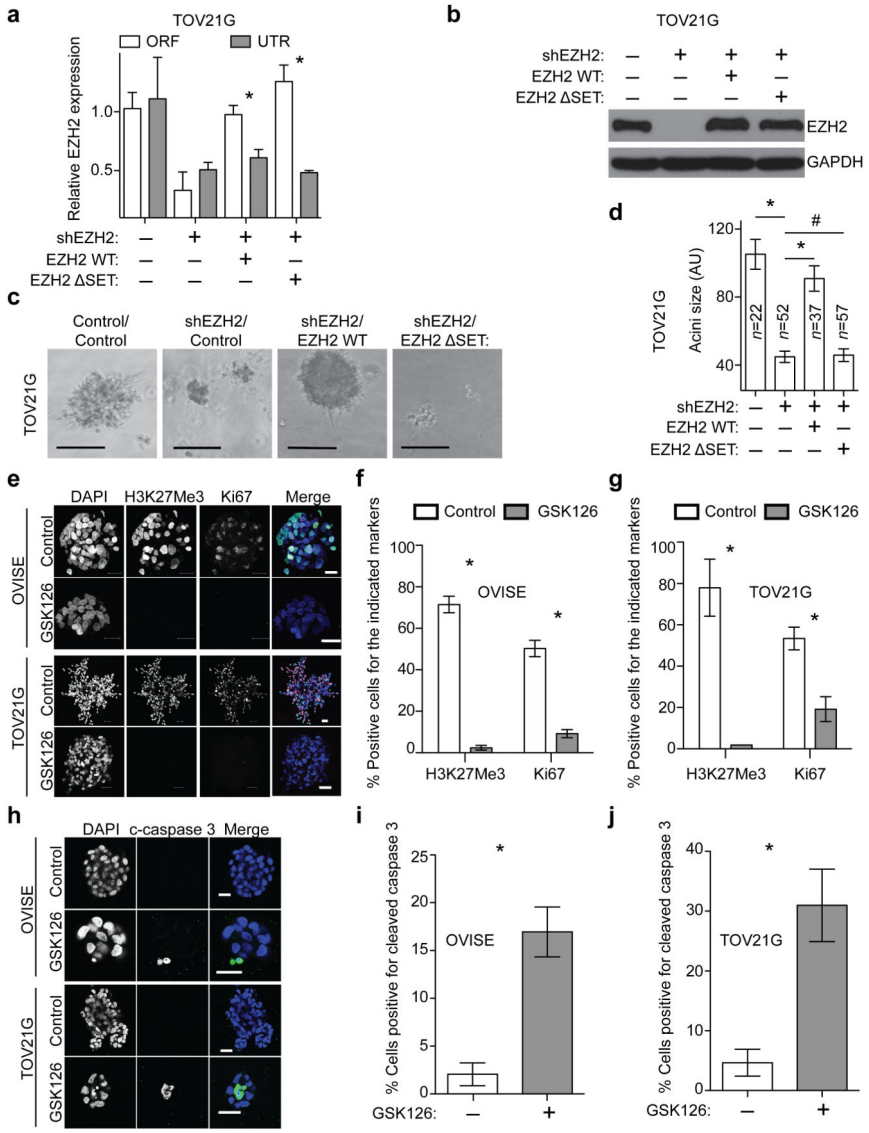

Figure 3.

EZH2 inhibitor triggers apoptosis of *ARID1A* mutated cells. (**a**) qRT-PCR analysis of *EZH2* untranslated region (UTR) and open reading frame (ORF) in TOV21G cells expressing a UTR targeting shEZH2 together with a wild type EZH2 or a SET domain deleted EZH2 mutant (EZH2 ΔSET). *n*=3, * *P*<0.01. (**b**) Immunoblotting of EZH2 and GAPDH in the indicated cells. (**c**) Images of acini formed in 3D culture for 12 days. Scale bars = 75 AU in NIH image J software. (**d**) Quantification of (c), **P*<0.01 and #*P*>0.05. (**e**) Immunofluorescence staining of Ki67 (red), H3K27Me3 (green) and DAPI (blue) for acini formed by *ARID1A* mutated OVISE and TOV21G cells cultured in 3D treated with 5 μM GSK126 or vehicle control for 12 days. Scale bars = 25μM. Note the different scale bars in different panels due to growth suppression by GSK126 treatment. (**f-g**) Quantification of (e). 200 cells from each of the indicated groups were examined for expression of Ki67 and H3K27Me3. *n*=3, 4, 5 and 4, **P* <0.01. (**h**) Same as (e), but stained for cleaved caspase 3 (green) and DAPI (blue) after 8 days of GSK126 treatment. Scale bars = 25μM. (**i-j**)

Quantification of (h). 200 cells from each of the indicated groups were examined for cleaved caspase 3 positivity. n=6 and 5,* P <0.01. Number of acini (n) is indicated on the graphs as the representative of three experimental repeats. Error bars represent s.e.m. P calculated with two-tailed t test.

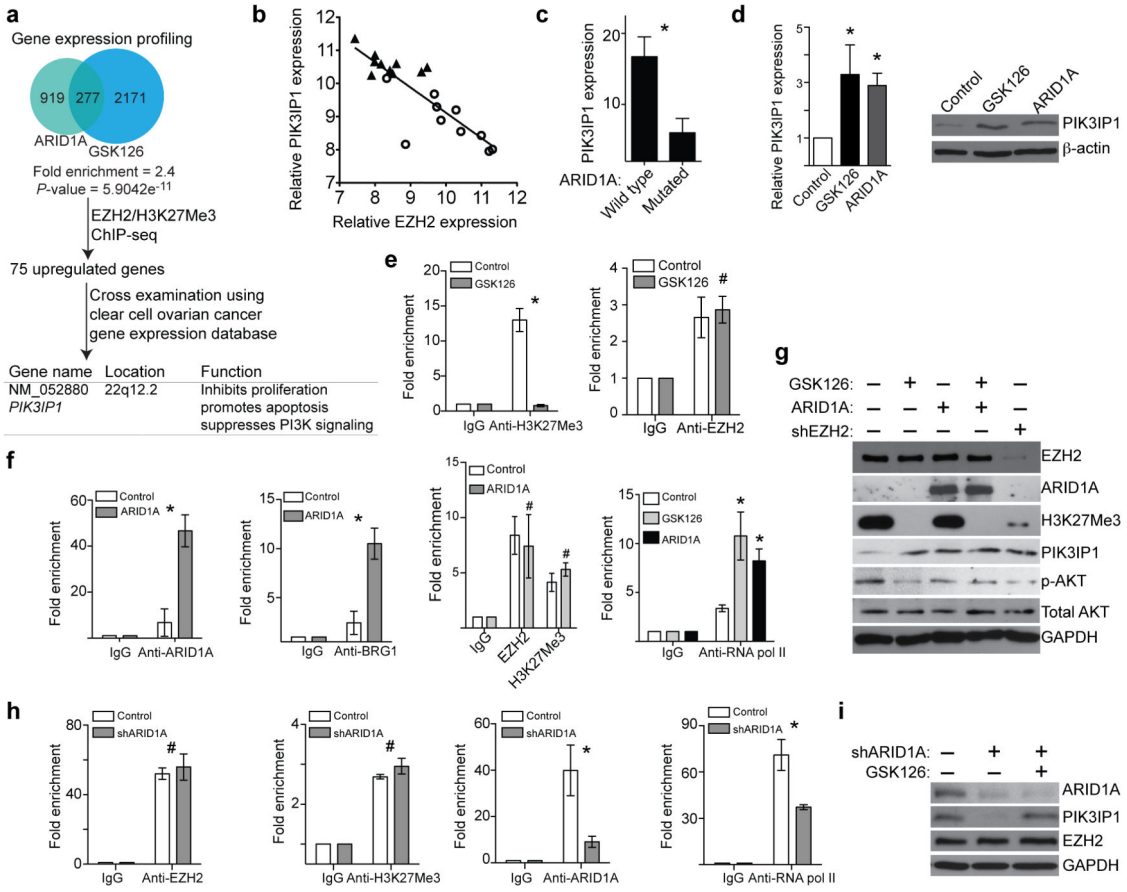

Figure 4.

PIK3IP1 is a novel ARID1A/EZH2 direct target gene. (**a**) Flow-diagram of the strategies used for identifying *PIK3IP1* as a direct ARID1A/EZH2 target gene. (**b**) Spearman statistical analysis of *PIK3IP1* and *EZH2* expression. Scatter plot of relative expression of *EZH2* (x-axis) and *PIK3IP1* (y-axis) from laser-capture and microdissected normal ovarian epithelium (*n*=10; triangles) and OCCCs (*n*=10; circles). (Spearman correlation r=-0.8211 and *P*<0.0001). (**c**) Relative *PIK3IP1* mRNA expression in *ARID1A* mutated (*n*=4) and wild type (*n*=5) OCCCs. * *P*=0.0207. (**d**) qRT-PCR analysis of *PIK3IP1* (*n*=4; * *P*<0.01) and immunoblotting of PIK3IP1 and β-actin in the indicated *ARID1A* mutated OVISE cells. (**e**) ChIP analysis of OVISE cells treated with vehicle control or 5 μM GSK126 using antibodies against H3K27Me3 or EZH2 for the *PIK3IP1* gene promoter. (*n*=3, * *P*<0.001, # *P*=0.9405). (**f**) ChIP analysis of *ARID1A* mutated OVISE cells with or without ARID1A restoration using the indicated antibodies or IgG control for the *PIK3IP1* gene promoter (*n*=3; # *P*>0.05; **P*<0.05). (**g**) Immunoblotting of the indicated proteins in *ARID1A* mutated TOV21G cells with or without ARID1A restoration treated with or without GSK126 (5μM) or expressing shEZH2. (**h**) ChIP analysis of *ARID1A* wild type RMG1 cells expressing control or shARID1A using the indicated antibodies or IgG control for the *PIK3IP1* gene promoter (*n*=3; # *P*>0.05; **P*<0.01). (**i**) Immunoblotting of the indicated proteins in *ARID1A* wild type RMG1 cells expressing control or shARID1A treated with or without 5μM

GSK126. Error bars represent s.e.m. *P* calculated with two-tailed *t* test except **a** using Spearman's test.

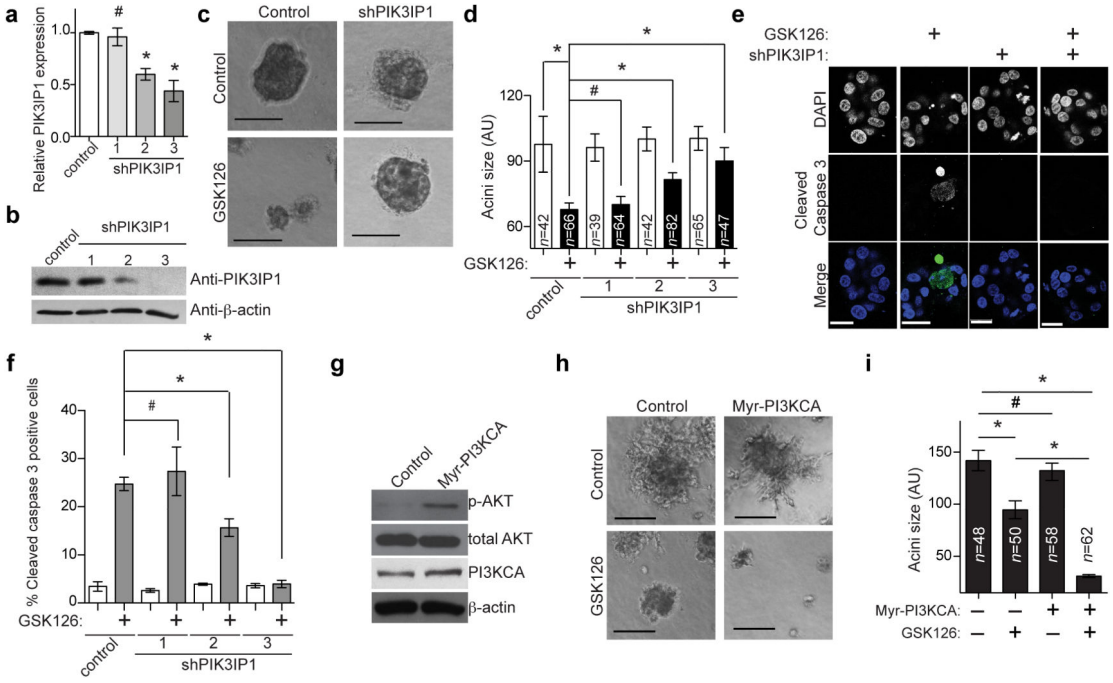

Figure 5.

PIK3IP1 contributes to the observed synthetic lethality. (**a**) qRT-PCR analysis of *PIK3IP1* mRNA in *ARID1A* mutated OVISE cells infected with lentivirus encoding the indicated shPIK3IP1s or controls. (n=3, # P=0.8149, *P<0.001). (**b**) Immunoblotting of PIK3IP1 and β-actin in the indicated OVISE cells. (**c**) Phase-contrast images of the indicated control or shPIK3IP1 (#3)-expressing OVISE cells treated with or without 5μM GSK126 for 12 days in 3D culture. (**d**) Quantification of (c). # P=0.628, *P<0.01. (**e**) Immunofluorescence staining for the apoptotic marker cleaved caspase 3 (green) in the acini formed by the indicated cells. Shown is shPIK3IP1 #3. Bars = 25 μm. (**f**) Quantification of (e). n=3, # P=0.642, * P<0.05. (**g**) Immunoblotting of phospho-AKT (p-AKT) and the indicated proteins in *ARID1A* mutated, *PI3KCA* wild type OVTOKO cells expressing a constitutively active myristoylated *PI3KCA* (I143V) mutant (Myr-PI3KCA) or controls. (**h**) Phase-contrast images of the indicated cells treated with or without 5μM GSK126 for 12 days in 3D culture. (**i**) Quantification of (h). # P>0.05 and * P<0.001. Number of acini (n) is indicated on the graphs as the representative of three experimental repeats. Error bars represent s.e.m. P calculated with two-tailed t test.

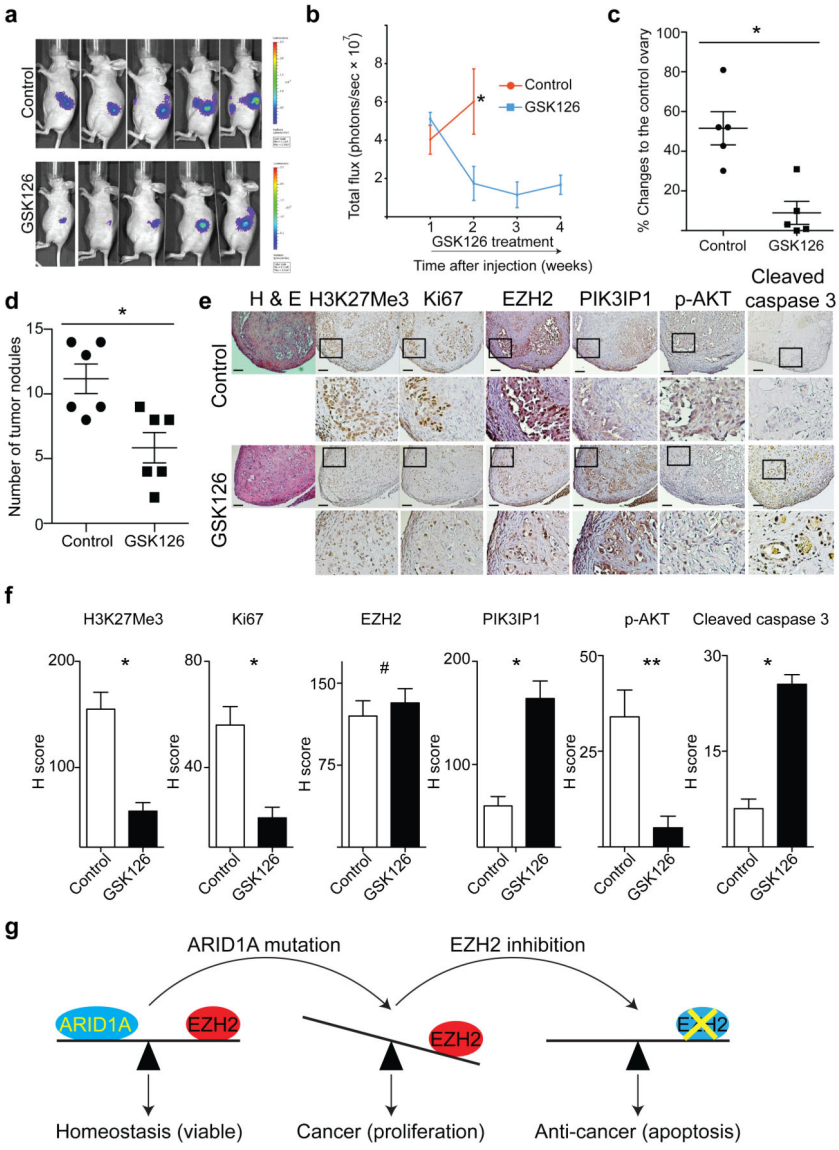

Figure 6.

EZH2 inhibitor causes the regression and reduces the number of tumor nodules of *ARID1A* mutated OCCC tumors. (**a**) 1×10^6 luciferase expressing *ARID1A* mutated OVISE cells were unilaterally injected into the bursa sac of the immuno-compromised female mice. The mice were randomized into two groups based on total luciferase flux for daily 50 mg/kg GSK126 or vehicle control treatments by intraperitoneal injection after 7 days. Mice were imaged every 7 days, and shown are images taken at day 14. (**b**) Quantification of tumor growth. n=5 and * P=0.0026. (**c**) At necropsy, the size of the dissected tumors was measured by subtracting control counter lateral ovary size from that of the size from the tumor cell injected one. n=5 and * P=0.003. (**d**) 3×10^6 *ARID1A* mutated OVISE cells were injected into the intraperitoneal cavity of immuno-compromised female mice. Mice were randomly separated into two groups after 4 days for daily 50 mg/kg GSK126 or vehicle control treatments. On day 30, the number of tumor nodules in intraperitoneal cavity were assessed. n=6 and * P=0.008). (**e**) Immunohistochemical staining using the indicated antibodies for

tumors dissected from GSK126 or control treated mice (magnification, 10X and 40X). Bars= 50 μm. (**f**) H-score quantification of (e). *n*=13 different fields from 5 different tumors. * *P*=0.0001; ** *P*=0.012 and # *P*=0.547. (**g**) A proposed model for the observed synthetic lethality between *ARID1A* mutation and inhibition of EZH2 methyltransferase activity. Error bars represent s.e.m. *P* calculated with two-tailed *t* test.